1164 *Chem. Mater.* **2010,** *22,* 1164–1172
DOI:10.1021/cm902593n

CHEMISTRY OF MATERIALS
Article

Synthesis, Characterization, and Thermal Stability of $LiNi_{1/3}Mn_{1/3}Co_{1/3-z}Mg_zO_2$, $LiNi_{1/3-z}Mn_{1/3}Co_{1/3}Mg_zO_2$, and $LiNi_{1/3}Mn_{1/3-z}Co_{1/3}Mg_zO_2$†

Wenbin Luo,[‡,§] Fu Zhou,[‡] Xuemei Zhao,[‡] Zhonghua Lu,[⊥] Xinhai Li,[§] and J.R. Dahn*[,‡]

[‡]*Department of Physics and Atmospheric Science, Dalhousie University, Halifax, B3H3J5, Canada,* [§]*School of Metallurgical Science and Engineering, Central South University, Changsha 410083, PR China, and* [⊥]*3M Co., 3M Center, St. Paul, Minnesota 55144-1000*

Received August 22, 2009. Revised Manuscript Received November 15, 2009

$LiNi_{1/3}Mn_{1/3}Co_{1/3-z}Mg_zO_2$, $LiNi_{1/3-z}Mn_{1/3}Co_{1/3}Mg_zO_2$, and $LiNi_{1/3}Mn_{1/3-z}Co_{1/3}Mg_zO_2$ ($0 \le z \le 1/3$) were prepared from hydroxide precursors. The hydroxide precursors were heated with Li_2CO_3 at 900 °C to prepare the oxides. Rietveld refinements of XRD data show that Mg substitution for Co, Ni and Mn results in different degrees of cation mixing in the Li layer with very little cation mixing in $LiNi_{1/3}Mn_{1/3-z}Co_{1/3}Mg_zO_2$ and the most cation mixing in $LiNi_{1/3}Mn_{1/3}Co_{1/3-z}Mg_zO_2$. Electrochemical studies of the $LiNi_{1/3}Mn_{1/3}Co_{1/3-z}Mg_zO_2$, $LiNi_{1/3-z}Mn_{1/3}Co_{1/3}Mg_zO_2$, and $LiNi_{1/3}Mn_{1/3-z}Co_{1/3}Mg_zO_2$ ($0 \le z \le 1/3$) samples were used to measure the rate of capacity reduction with Mg content, found to be about -389 (mAh/g)/($z = 1$) independent of which cation was substituted by Mg. The impact of Mg substitution on the thermal stability of NMC samples was studied via accelerating rate calorimetry and compared with Al-substituted NMC samples. The substitution of Mg did not improve the thermal stability of the samples, independent of which cation was substituted and independent of the amount of Mg added, in contrast to the effect of Al, which dramatically improves thermal stability.

1. Introduction

Dahn's group and Ohzuku's group reported the structure and electrochemical performance of $Li[Ni_xMn_xCo_{1-2x}]O_2$ with x either approximately equal to 1/3 or equal to 1/3.[1,2] Much research has been performed to optimize this and similar materials by new synthesis methods, applying coatings and including substituents for Ni, Mn, or Co.

The impact of Al substitutions on the structure, electrochemical, and thermal properties of layered lithium transition metal oxides is well-known.[3−7] Reports about the effects of Mg substitutions on the properties of layered positive electrode materials are less common. Tukamoto and West reported the conductivity of $LiCoO_2$ at room temperature can be increased by partial substitution of Co^{3+} by Mg^{2+}.[8] Levasseur and Delmas further confirmed the results by Tukamoto and West. They found that Mg substitution could enhance the structural stability upon cycling.[9] Luo and Dahn carefully studied the crystal chemistry and electrochemical properties of $Li[Co_{1-z}Mg_z]O_2$ and $Li_{1-z}Mg_z[Co_{1-z}Mg_z]O_2$.[10] Cho et al. synthesized $LiNi_{0.74}Co_{0.26-x}Mg_xO_2$ using a coprecipitaion method. They found that the exothermic peak from the reaction of charged $LiNi_{0.74}Co_{0.26-x}Mg_xO_2$ with electrolyte, as measured by DSC, was significantly smaller than that of $LiNi_{0.74}Co_{0.26}O_2$ for $x > 0.04$, suggesting that Mg substitution improved the thermal stability of the electrode material.[11] Kim and Sun showed that Mg-substitution for Mn in $Li[Ni_{1/3}Mn_{1/3}Co_{1/3}]O_2$ improved the capacity, cyclability, and thermal stability.[12] Duh et al. reported that Mg-substituted $LiNi_{0.57}Mg_{0.03}Co_{0.25}Mn_{0.15}O_2$ showed better capacity retention than materials without Mg. They also found that $LiNi_{0.57}Mg_{0.03}Co_{0.25}Mn_{0.15}O_2$ also showed an increase in thermal stability compared to samples without Mg.[13]

Much of the work in the literature has been reported for only a few samples, not systematic series of samples from which trends, if any, can be clearly observed. When only a few samples are studied, it is possible that spurious conclusions can be reached. In this work, the synthesis, structure, and electrochemical properties of $LiNi_{1/3}Mn_{1/3}Co_{1/3-z}Mg_zO_2$, $LiNi_{1/3-z}Mn_{1/3}Co_{1/3}Mg_zO_2$, $LiNi_{1/3}Mn_{1/3-z}Co_{1/3}Mg_zO_2$

†Accepted as part of the 2010 "Materials Chemistry of Energy Conversion Special Issue".

*Corresponding author e-mail address: jeff.dahn@dal.ca.

(1) Lu, Z. H.; MacNeil, D. D.; Dahn, J. R. *Electrochem. Solid-State Lett*. **2001**, *4*, A200.
(2) Ohzuku, T.; Makimura, Y. *Chem. Lett*. **2001**, 642.
(3) Ohzuku, T.; Ueda, A.; Kouguchi, M. *J. Electrochem. Soc*. **1995**, *142*, 4033.
(4) Ceder, G.; Chiang, Y. M.; Sadoway, D. R.; Aydinol, M. K.; Jang, Y. I.; Huang, B. *Nature* **1998**, *392*, 694.
(5) Luo, W. B; Dahn, J. R. *Chem. Mater*. **2009**, *21*, 56.
(6) Luo, W. B; Dahn, J. R. *Electrochim. Acta* **2009**, *54*, 4655.
(7) Zhou, F.; Zhao, X. M; Lu, Z. H; Jiang, J. W.; Dahn, J. R. *Electrochem. Commun*. **2008**, *10*, 1168.
(8) Tukamoto, H.; West, A. R. *J. Electrochem. Soc*. **1997**, *144*, 3164.
(9) Levasseur, S.; Menetrier, M.; Delmas, C. *Chem. Mater*. **2002**, *14*, 3584.
(10) Luo, W. B.; Dahn, J. R. J. Electrochem. Soc., in press.
(11) Cho, J. *Chem. Mater*. **2000**, *12*, 3089.
(12) Kim, G. H.; Myung, S. T.; Kim, H. S.; Sun, Y. K. *Electrochim. Acta* **2006**, *51*, 2447.
(13) Liao, P. Y.; Duh, J. G.; Sheu, H. S. *J. Power Source* **2008**, *183*, 766.

 Published on Web 12/10/2009

($0 \leq z \leq 1/3$) are characterized carefully. In addition, the reactivity of the charged electrode materials with electrolyte is measured using accelerating rate calorimetry.

2. Experimental Section

2.1. Material Preparation. A $LiOH \cdot H_2O$ (Sigma Aldrich, 98%+) solution and a mixed solution of $Ni(NO_3)_2 \cdot 6H_2O$(Sigma Aldrich, 97%+), $Mn(NO_3)_2 \cdot 4H_2O$(Sigma Aldrich, 97%+), $Co(NO_3)_2 \cdot 6H_2O$(Sigma Aldrich, 98%+), and $Mg(NO_3)_2 \cdot 6H_2O$ (Sigma Aldrich, 98%+) were simultaneously added over the course of about 30 min to a stirred flask using a two-channel peristaltic pump (Masterflex C/L pump, Barnant Co.). The concentrations of the solutions were adjusted to set the Mg/(Ni + Mn + Co + Mg) ratio, z. The precipitate was separated by centrifuging (Centra GP8R, International equipment company) and was washed with distilled water several times to remove any dissolved salts, then was dried at 80 °C overnight. The PH of the washing water was 6.9. The dried precipitate was mixed with an appropriate amount of Li_2CO_3 (Alfa Aesar, 99%) and ground using an automatic grinder (Retsch RM-0). The precursors were heated in air at 900 °C for 3 h.

2.2. Material Characterization. *2.2.1. X-ray Diffraction.* XRD patterns were collected with a Siemens D5000 diffractometer equipped with a Cu target X-ray tube and a diffracted beam monochromator. The $LiNi_{1/3}Mn_{1/3}Co_{1/3-z}Mg_zO_2$, $LiNi_{1/3-z}Mn_{1/3}Co_{1/3}Mg_zO_2$, and $LiNi_{1/3}Mn_{1/3-z}Co_{1/3}Mg_zO_2$ ($0 \leq z \leq 1/3$) samples were measured over a scattering angle range between 10 and 90° using 0.05° steps and a 30 s counting time. This long counting time was used so that small amounts of impurity phases could be detected.

2.2.2. Atomic Absorption Analysis. Atomic absorption spectroscopy performed at the Minerals Engineering Center at Dalhousie University was used to measure the Mg/(Ni + Mn + Co + Mg) and Li/(Ni + Mn + Co + Mg) ratio in the heat-treated oxide. The procedures used have been shown to give a Li/Co ratio of 1.0:1.0 for stoichiometric $LiCoO_2$ samples obtained from battery materials suppliers.

2.2.3. SEM Testing. A Hitachi S4700 field-emission scanning electron microscope (SEM) was used to image the materials.

2.2.4. Electrochemical Testing. Coin cells (23 mm diameter and 2.5 mm thick) were used for testing the electrochemical performance of the samples. Positive electrodes were prepared by mixing the active material, Super S Carbon Black, and PVDF in a weight ratio of 90:5:5. An appropriate amount of NMP was added to the mixture to form a slurry, which was then thoroughly mixed. The slurry was coated on Al foil and dried overnight in an oven. The electrochemical cells used a single lithium metal foil used as the counterelectrode, Celgard 2320 microporous film as the separator, and 1 M $LiPF_6$ in ethylene carbonate (EC) and diethyl carbonate (DEC) (1:2,v/v) as the electrolyte. Cells were assembled in an argon-filled glovebox. The cells were removed from the glovebox and connected to a computer-controlled charging system (E-One/Moli Energy). The cells were initially charged and discharged at a C/20 rate between 3.3 and 4.3 V vs Li metal for two cycles. After the first two cycles, the charge−discharge rate was increased to C/5.

2.2.5. Thermal Stability Testing by Accelerating Rate Calorimetry. The thermal stability of as-prepared Mg-substituted NMC samples were tested using accelerating rate calorimetry (ARC). ARC sample preparation methods are the same as reported in our earlier works.[14−16] Pellet coin cells were made and charged to 4.3 V using the protocol described in ref 7. Then the cells were opened in an argon-filled glovebox and the electrode powder was rinsed with DMC four times and dried in the glovebox as described in ref 15. Charged cathode material (94 mg) and 30 mg of 1 M $LiPF_6$ EC/DEC electrolyte were used for the ARC tests. The ARC starting temperature was set to either 70 or 180 °C. Exothermic reactions were tracked under adiabatic conditions when the sample SHR exceeded 0.03 °C/min. Experiments were stopped at 350 °C or when the self-heating rate, SHR, was higher than 20 °C/min.

3. Results and Discussion

Figure 1 shows the XRD patterns of all the $LiNi_{1/3}Mn_{1/3}Co_{1/3-z}Mg_zO_2$, $LiNi_{1/3-z}Mn_{1/3}Co_{1/3}Mg_zO_2$, and $LiNi_{1/3}Mn_{1/3-z}Co_{1/3}Mg_zO_2$ samples in the scattering angle range between 10 and 90°. The left column shows the patterns for the $LiNi_{1/3}Mn_{1/3}Co_{1/3-z}Mg_zO_2$ samples. The center column shows the patterns for the $LiNi_{1/3-z}Mn_{1/3}Co_{1/3}Mg_zO_2$ samples and the right column shows the patterns for the $LiNi_{1/3}Mn_{1/3-z}Co_{1/3}Mg_zO_2$ samples. To observe the characteristic peaks clearly, expanded views of the (101), (006), (012), (018), (110), and (113) Bragg peaks are given in Figures 2−4. In addition, an expanded view, on a sensitive vertical scale, is given of the region where impurities like Li_2CO_3 are known to appear.

Figure 2 shows XRD patterns of the $LiNi_{1/3}Mn_{1/3}Co_{1/3-z}Mg_zO_2$ ($0 \leq z \leq 1/3$) samples synthesized at 900 °C. All of the peaks can be indexed based on a hexagonal α-$NaFeO_2$ structure (space group $R3\bar{M}$). The left panels in Figure 2 show the portion of the XRD pattern where the Li_2CO_3 impurity appears for the samples with $z \geq 0.2$. The center panels and the right panels in Figure 1 show the separation between the (006)/(012) and the (108)/(110) peaks decreases as the Mg content increases. The results in Figure 2 suggest that single phase samples can be prepared under these conditions at least for $0 \leq x < 0.2$. Even though some Li_2CO_3 impurity appears for $z \geq 0.2$, the 110 and 113 peaks are clearly shifting over this composition range suggesting that the single phase range extends to higher compositions than $z = 0.2$. Longer heating times or intermediate grindings, followed by a second heating, may be required to make completely pure samples in this range of composition.

Figure 3 shows XRD patterns of $Li[Ni_{1/3-z}Mn_{1/3}Co_{1/3}Mg_z]O_2$ ($0 \leq z \leq 1/3$) synthesized at 900 °C. A broad weak XRD peak (indicated by the triangle) around 20.7° is presumably caused by the short-range ordering of Li, Ni, Co, Mn, and Mg in the transition-metal layers for $z \geq 0.25$. The separation between the 012/006 and 018/100 peaks remains as Mg is substituted for Ni (Figure 3) unlike the case when Mg is substituted for Co (Figure 2) where the peaks merge the Mg content increases. Single-phase $Li[Ni_{1/3-z}Mn_{1/3}Co_{1/3}Mg_z]O_2$ samples can be prepared for $0 \leq z \leq 1/3$.

(14) Wang, Y.; Jiang, J.; Dahn, J. R. *Electrochem. Commun.* **2007**, *9*, 2534.
(15) Wang, Y.; Zaghib, K.; Guerfi, A.; Bazito, F. F. C.; Torresi, R. M.; Dahn, J. R. *Electrochim. Acta* **2007**, *52*, 6234.
(16) Richard, M. N.; Dahn, J. R. *J. Electrochem. Soc.* **1999**, *146*, 2068.

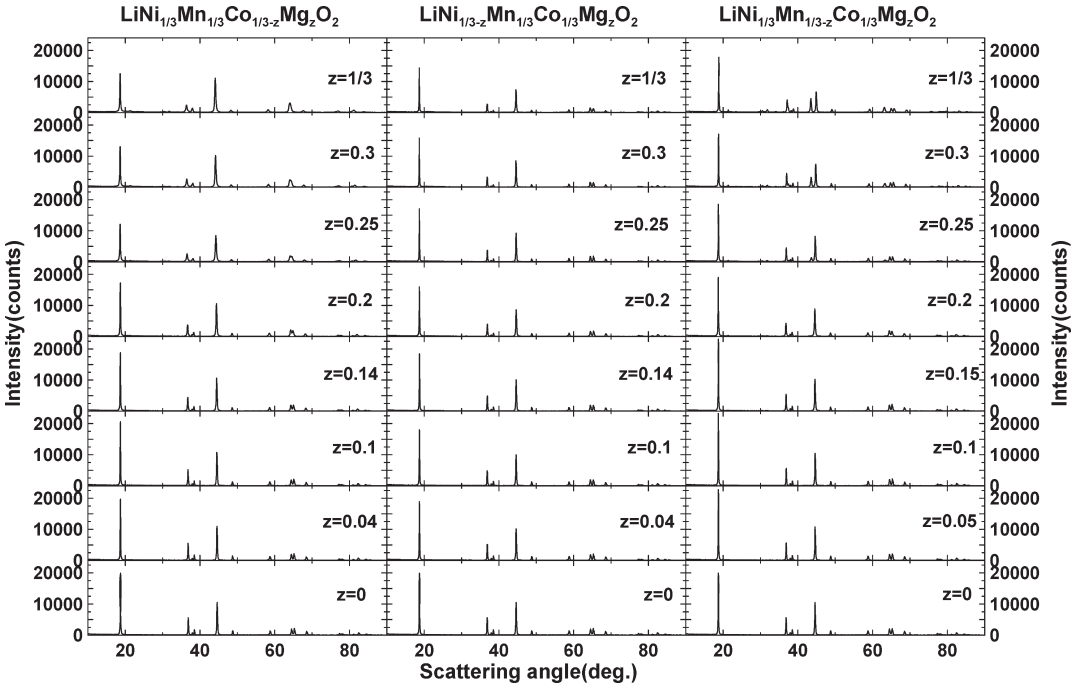

Figure 1. XRD patterns of $LiNi_{1/3}Mn_{1/3}Co_{1/3-z}Mg_zO_2$ (left panels), $LiNi_{1/3-z}Mn_{1/3}Co_{1/3}Mg_zO_2$ (center panels), and $LiNi_{1/3}Mn_{1/3-z}Co_{1/3}Mg_zO_2$ (right panels).

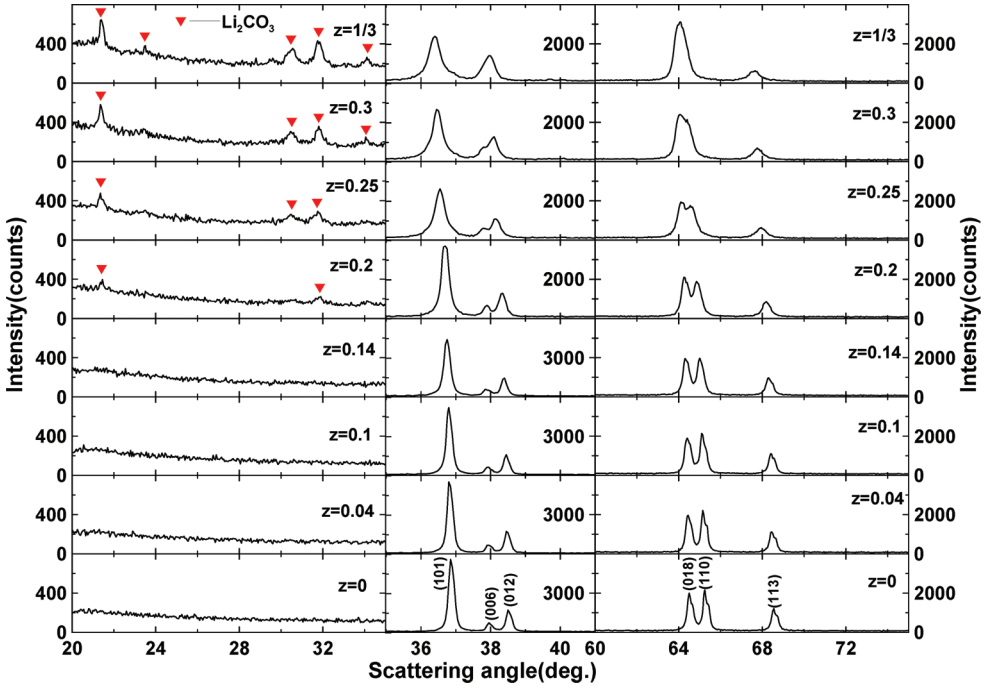

Figure 2. XRD patterns of $LiNi_{1/3}Mn_{1/3}Co_{1/3-z}Mg_zO_2$ (20°−35°, 35°−41°, 60°−75°). Notice the change of vertical scale from panel to panel.

Figure 4 shows XRD patterns of $LiNi_{1/3}Mn_{1/3-z}Co_{1/3}Mg_zO_2$ ($0 \leq z \leq 1/3$) synthesized at 900 °C. The left panels in Figure 4 show the appearance of a Li_2CO_3 impurity for the $z \geq 0.2$ samples. By comparison with Figure 1, the amount of Li_2CO_3 is much larger when Mg is substituted for Mn than when it is substituted for Co. The center panels and the right panels in Figure 4 show the appearance of a rock-salt-type impurity as evidenced by the Bragg peaks at around 37.5° and 63°. The results in Figure 4 suggest that single phase samples can be prepared under these conditions for $0 \leq x < 0.2$.

Figure 5 shows the lattice constants (a and c) as a function of z in $LiNi_{1/3}Mn_{1/3}Co_{1/3-z}Mg_zO_2$, $LiNi_{1/3-z}Mn_{1/3}Co_{1/3}Mg_zO_2$, and $LiNi_{1/3}Mn_{1/3-z}Co_{1/3}Mg_zO_2$ ($0 \leq z \leq 1/3$) for the samples described by Figures 2−4. The lattice constants were determined by least-squares refinements to the measured positions of at least 10 Bragg peaks. The left panels show the variation in the lattice

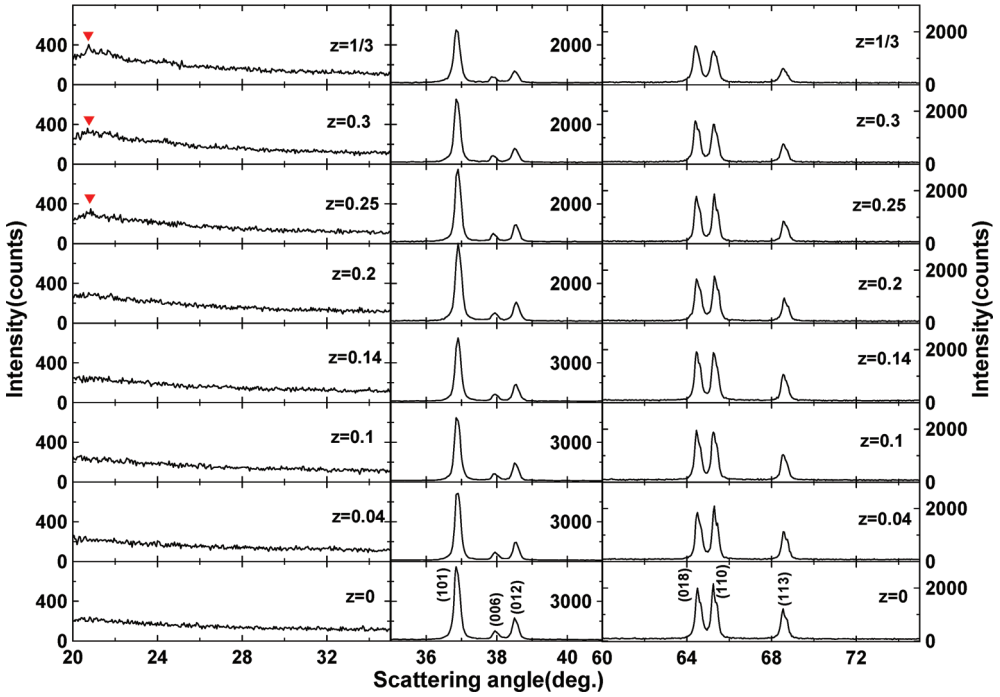

Figure 3. XRD patterns of $LiNi_{1/3-z}Mn_{1/3}Co_{1/3}Mg_zO_2$ (20°−35°, 35°−41°, 60°−75°). Notice the change of vertical scale from panel to panel.

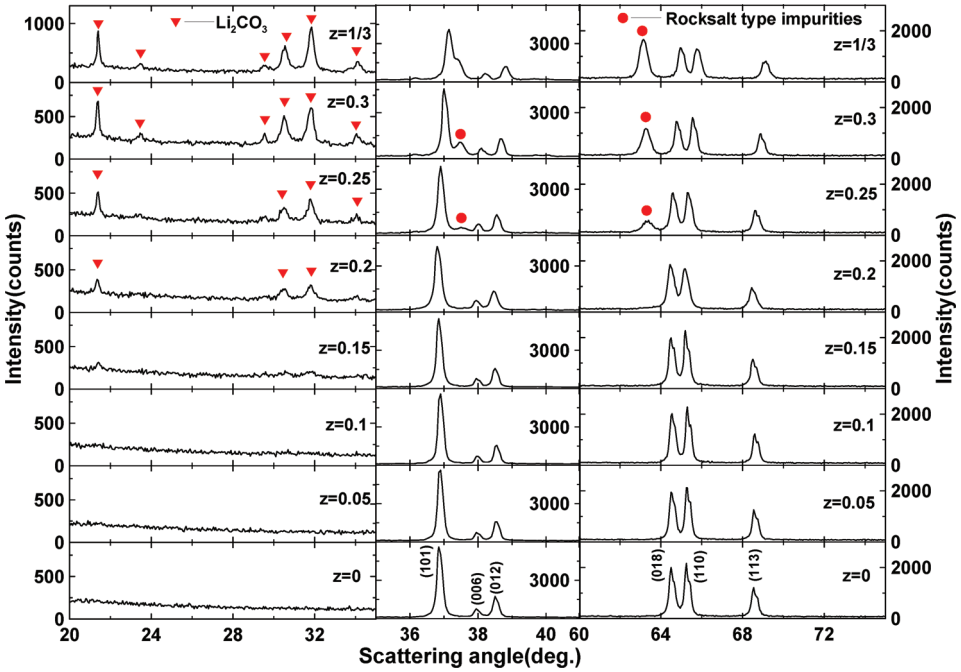

Figure 4. XRD patterns of $LiNi_{1/3}Mn_{1/3-z}Co_{1/3}Mg_zO_2$ (20°−35°, 35°−41°, 60°−75°). Notice the change of vertical scale from panel to panel.

parameters, a and c, for $LiNi_{1/3}Mn_{1/3}Co_{1/3-z}Mg_zO_2$. To qualitatively understand the lattice parameter variations, the initial oxidation states of the cations in $LiNi_{1/3}Mn_{1/3}Co_{1/3}O_2$, must be given. These are Ni^{2+}, Co^{3+}, and Mn^{4+}.[1] Both lattice constants increase with z since the ionic radius of Mg^{2+} is larger than that of Co^{3+} and Co^{4+} ions ($r_{Mg}{}^{2+}$ = 0.72 Å, $r_{Co}{}^{3+}$ = 0.545 Å, $r_{Co}{}^{4+}$ = 0.53 Å).[17] The center panels in Figure 5 show the variation of the lattice constants a and c of the $LiNi_{1/3-z}Mn_{1/3}Co_{1/3}Mg_zO_2$ samples for $0 \le z \le 1/3$. The lattice constant, a, is almost constant, and c varies weakly as z varies when Mg is substituted for Ni. This is presumably because the size of Ni^{2+} and Mg^{2+} are almost the same ($r_{Mg}{}^{2+}$ = 0.72 Å, $r_{Ni}{}^{2+}$ = 0.69 Å).[17] The right panels in Figure 5 show the variation of the lattice constants, a and c, of the $LiNi_{1/3}Mn_{1/3-z}Co_{1/3}Mg_zO_2$ series for $0 \le z \le 1/3$, bearing in mind that the samples are not pure for $z > 0.15$. The lattice constants, a and c, are basically constant in the single phase region (up to $z = 0.15$). This lack of variation is counterintuitive because the ionic radius of Mg^{2+} is larger than Mn^{4+}

(17) Shannon, R. D. *Acta Crystallogr.* **1976**, *A32*, 751–767.

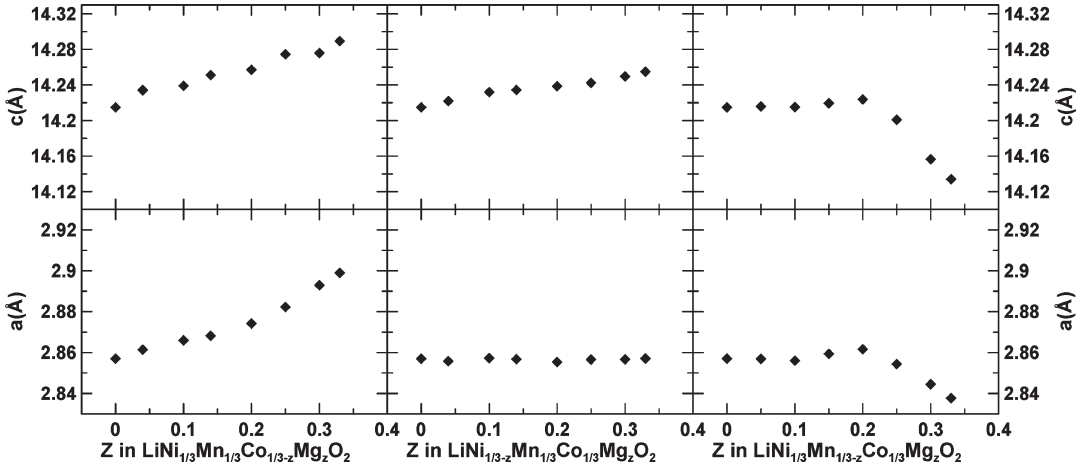

Figure 5. Lattice constants of $LiNi_{1/3}Mn_{1/3}Co_{1/3-z}Mg_zO_2$, $LiNi_{1/3-z}Mn_{1/3}Co_{1/3}Mg_zO_2$, and $LiNi_{1/3}Mn_{1/3-z}Co_{1/3}Mg_zO_2$ versus Mg content ($0 \leq z \leq 1/3$).

(r_{Mg}^{2+} = 0.72 Å, r_{Mn}^{4+} = 0.53 Å).[17] But some Ni^{2+} will become Ni^{3+} when Mg^{2+} substitute Mn^{4+}, the ionic radius of Ni^{3+} is smaller than Ni^{2+}(r_{Ni}^{2+} = 0.69 Å, r_{Ni}^{3+} = 0.56 Å).[17] Therefore, the lattice constant almost keep unchanged when Mg^{2+} substitute Mn^{4+}. The lattice constant, *a* and *c*, decrease rapidly for $z > 0.2$ because of undesired composition changes resulting from the presence of the rocksalt impurity phase (see Figure 4).

To further understand the influence of the Mg substitution on the structure of these materials, Rietveld refinements were carried out for all samples. We assume Li on 3a sites, Ni, Mn, Co, and Mg on 3b sites, and oxygen on 6c sites. The refinements allow for a small amount of transition metal atoms (presumably Ni) on the 3b sites (in the transition metal layer) to exchange with Li on the 3a sites (in the Li layer). Our previous studies suggest that Mg can not enter the Li layer in the $Li[Co_{1-z}Mg_z]O_2$ system despite similar ionic radii (r_{Li}^{+} = 0.76 Å; r_{Mg}^{2+} = 0.72 Å).[10,17] Thus, the nominal formula of $LiNi_{1/3}Mn_{1/3}Co_{1/3-z}Mg_zO_2$, for example, is assumed to be as follows: $[Li_{1-x}Ni_x]_{3a}[Li_xNi_{1/3-x}Mn_{1/3}Co_{1/3-z}Mg_z]_{3b}O_2$. We emphasize that we can not be certain it is Ni that moves to the 3a sites. Pseudo-Voight peak shapes were used to describe the Bragg peaks.

Figure 6 shows the typical agreement between the observed and calculated XRD patterns using the $LiNi_{1/3}Mn_{1/3}Co_{0.23}Mg_{0.1}O_2$, $LiNi_{0.23}Mn_{1/3}Co_{1/3}Mg_{0.1}O_2$ and $LiNi_{1/3}Mn_{0.23}Co_{1/3}Mg_{0.1}O_2$, $LiNi_{1/3}Mn_{0.23}Co_{0.03}Mg_{0.3}O_2$ samples as examples. This suggests that the structural model is correct. The latter sample contained a Li_2CO_3 impurity, so a two-phase refinement was used. Li_2CO_3 structural parameters were fixed at literature values. Figure 7 shows the variation of transition metal content in the Li layers for the three sample series. For the unsubstituted $LiNi_{1/3}Mn_{1/3}Co_{1/3}O_2$ (NMC) sample, the transition metal content in the Li layer is 1.7% in good agreement with previous work.[18] When Mg substitutes for Co in NMC, there is strong increase in the amount of

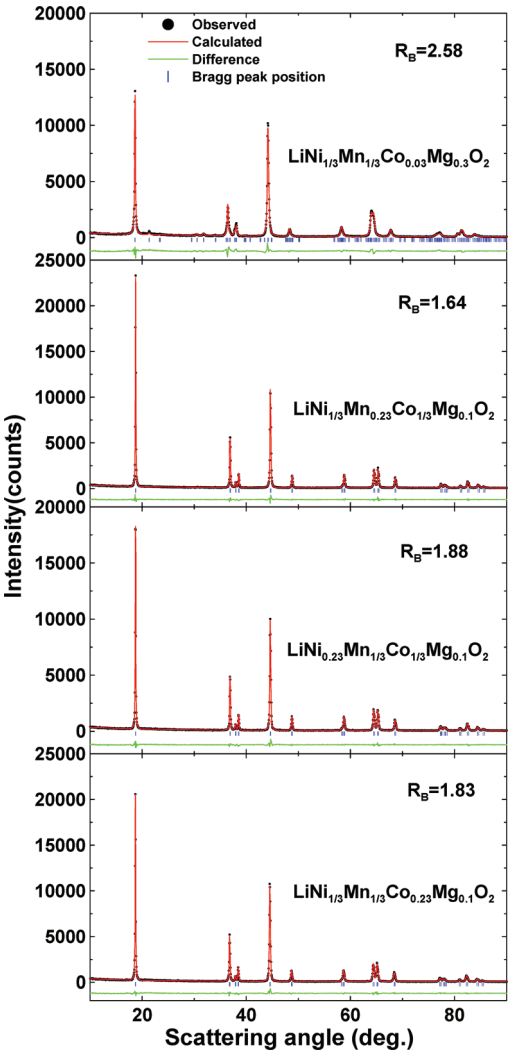

Figure 6. Rietveld refinement results for $LiNi_{1/3}Mn_{1/3}Co_{0.23}Mg_{0.1}O_2$, $LiNi_{0.23}Mn_{1/3}Co_{1/3}Mg_{0.1}O_2$, $LiNi_{1/3}Mn_{0.23}Co_{1/3}Mg_{0.1}O_2$, and $LiNi_{1/3}Mn_{1/3}Co_{0.03}Mg_{0.3}O_2$ samples.

transition metal in the Li layer. For the samples where Mg substitutes for Ni, there is a more modest increase in the transition metal content in the Li layer, while when Mg substitutes for Mn, there is no increase in transition metal

(18) MacNeil, D. D.; Lu, Z. H.; Dahn, J. R. *J. Electrochem. Soc.* **2002**, *149*, A1332.

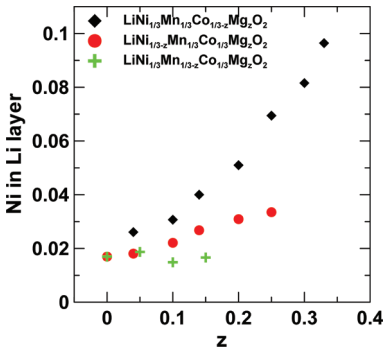

Figure 7. Transition metal content in the Li layer of $LiNi_{1/3}Mn_{1/3}Co_{1/3-z}Mg_zO_2$, $LiNi_{1/3-z}Mn_{1/3}Co_{1/3}Mg_zO_2$, and $LiNi_{1/3}Mn_{1/3-z}Co_{1/3}Mg_zO_2$ plotted versus Mg content; z obtained by Rietveld refinements.

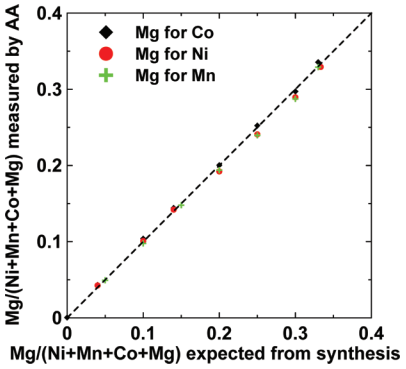

Figure 8. Mg/(Ni + Mn + Co + Mg) ratio measured by AA analysis plotted versus that expected from synthesis for all the $LiNi_{1/3}Mn_{1/3}Co_{1/3-z}Mg_zO_2$, $LiNi_{1/3-z}Mn_{1/3}Co_{1/3}Mg_zO_2$, and $LiNi_{1/3}Mn_{1/3-z}Co_{1/3}Mg_zO_2$ samples prepared in this work.

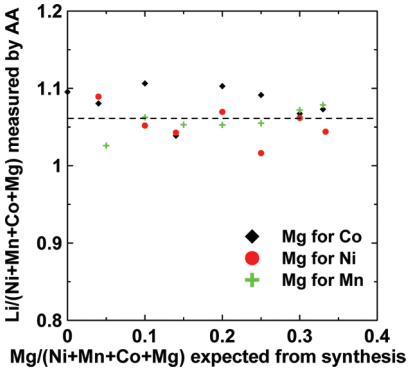

Figure 9. Li/(Ni + Mn + Co + Mg) ratio measured by AA analysis plotted versus that expected from synthesis for all the $LiNi_{1/3}Mn_{1/3}Co_{1/3-z}Mg_zO_2$, $LiNi_{1/3-z}Mn_{1/3}Co_{1/3}Mg_zO_2$, and $LiNi_{1/3}Mn_{1/3-z}Co_{1/3}Mg_zO_2$ samples prepared in this work.

in the Li layer with Mn content. Similar observations have been reported previously.[19]

Figure 8 shows the variation of the measured Mg content in the samples as measured by AA analysis compared to the expected content based on the molar ratios used during synthesis. The agreement is excellent, suggesting that the Mg is incorporated within the final oxide samples.

(19) Myung, S. T.; Komaba, S.; Hosoya, K.; Hirosaki, N.; Miura, Y.; Kumagai, N. *Chem. Mater.* **2005**, *17*, 2427.

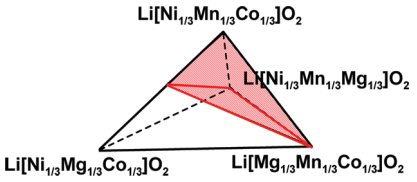

Figure 10. Schematic phase diagram of the $Li[Ni_{1/3}Mn_{1/3}Co_{1/3}]O_2$−$Li[Ni_{1/3}Mg_{1/3}Co_{1/3}]O_2$−$Li[Mg_{1/3}Mn_{1/3}Co_{1/3}]O_2$−$Li[Ni_{1/3}Mn_{1/3}Mg_{1/3}]O_2$ system designating the compositions that can be prepared as single phases (based on simple oxidation state rules) as the shaded region.

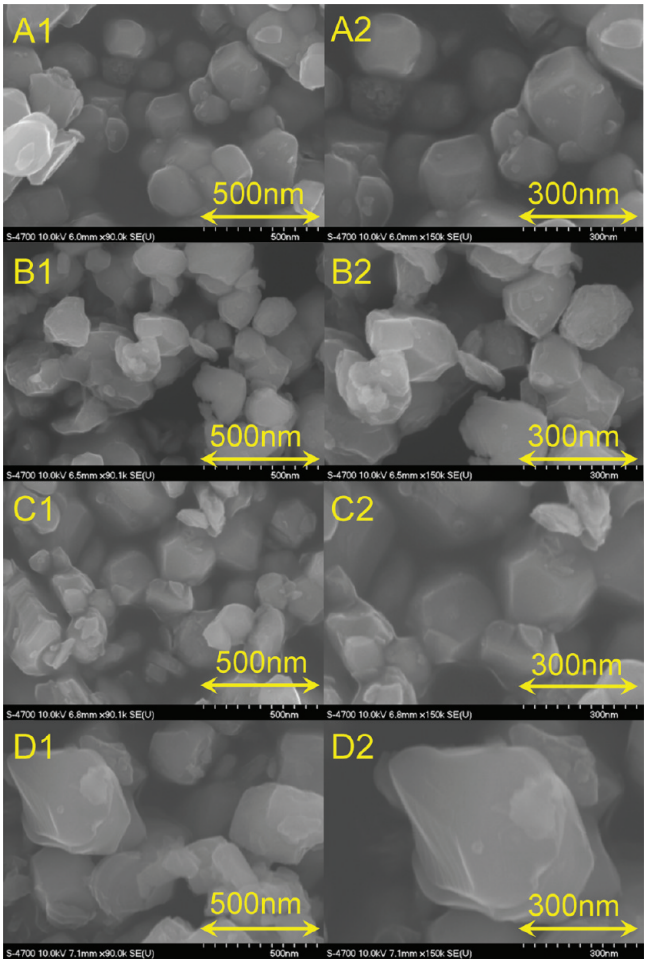

Figure 11. SEM images of (A) $LiNi_{1/3}Mn_{1/3}Co_{1/3}O_2$, (B) $LiNi_{1/3}Mn_{1/3}Co_{0.19}Mg_{0.14}O_2$, (C) $LiNi_{0.19}Mn_{1/3}Co_{1/3}Mg_{0.14}O_2$, and (D) $LiNi_{1/3}Mn_{0.18}Co_{1/3}Mg_{0.15}O_2$.

Figure 9 shows the variation of the measured Li content in the samples as measured AA analysis compared to the expected content based on the molar ratios used during synthesis. Figure 9 shows that Li content (the molar ratio of Li versus M (M = Ni + Mn + Co + Mg) ranged between 1.0 to 1.1. This lithium excess occurred because it was impossible to recover all the coprecipitate during the washing and centrifuging process. The amount of lithium added to the coprecipitate was based on an expected full recovery. It appears that typically, only about 95% of the hydroxide was recovered. The outcome of this result is that all of the samples are about 5% rich in lithium.

The predicted single-phase region for Mg-substituted NMC is schematically depicted by the shaded region in

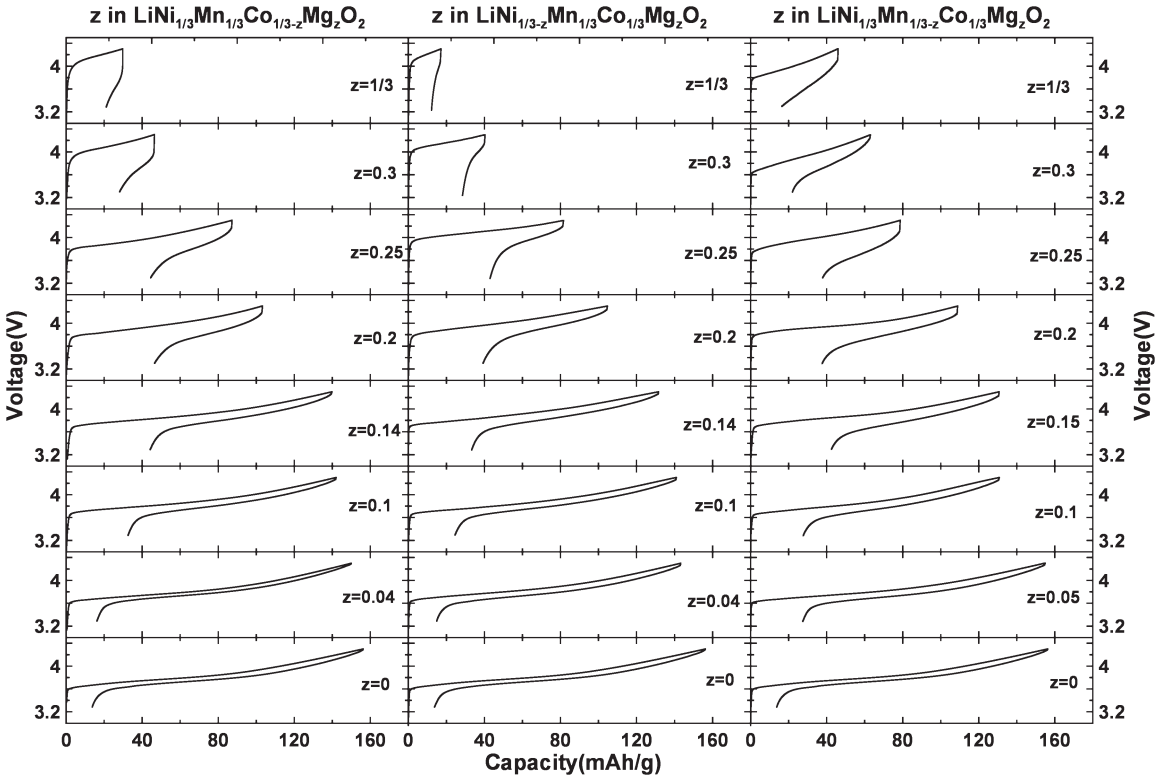

Figure 12. The potential (V) vs specific capacity (mAh/g) of Li/$LiNi_{1/3}Mn_{1/3}Co_{1/3-z}Mg_zO_2$, Li/$LiNi_{1/3-z}Mn_{1/3}Co_{1/3}Mg_zO_2$, and Li/$LiNi_{1/3}Mn_{1/3-z}Co_{1/3}Mg_zO_2$ ($0 \leq z \leq 1/3$) cells cycled between 3.3 and 4.3 V at a rate of C/20. Results for $LiNi_{1/3}Mn_{1/3}Co_{1/3-z}Mg_zO_2$, $LiNi_{1/3-z}Mn_{1/3}Co_{1/3}Mg_zO_2$, and $LiNi_{1/3}Mn_{1/3-z}Co_{1/3}Mg_zO_2$ ($0 \leq z \leq 1/3$) are shown in the left, center, and right panels, respectively.

Figure 10 and can be basically understood as follows. First, assume that the oxidation states of Mn and Co during heating in air in the presence of the other elements can only be Mn^{4+} and Co^{3+}. Assume that Ni prefers to be Ni^{2+}, but can be Ni^{3+}, and that Mg is always Mg^{2+}. Thus, the end members of the solid solution ranges should be $Li[Ni_{1/3}{}^{3+}Mn_{1/3}{}^{4+}Mg_{1/3}{}^{2+}]O_2$ when Mg is substituted for Co, $Li[Ni_{1/3}{}^{3+}Co_{1/3}{}^{3+}Mn_{1/6}{}^{4+}Mg_{1/6}{}^{2+}]O_2$, when Mg is substituted for Mn and $Li[Mn_{1/3}{}^{4+}Co_{1/3}{}^{3+}Mg_{1/3}{}^{2+}]O_2$, when Mg is substituted for Ni. The experimental observations we have made, along the edges of the tetrahedron in Figure 10, are consistent with the predictions of these simple oxidation state rules. In particular, Figure 10 predicts that the limit of the single phase region when Mg substitutes for Mn in $LiNi_{1/3}Mn_{1/3-z}Co_{1/3}Mg_zO_2$ should be $z = 1/6$, in good agreement with Figure 4.

Figure 11 shows scanning electron micrographs of four of the samples studied here. Figures 11A1 and A2 show the morphology of the $LiNi_{1/3}Mn_{1/3}Co_{1/3}O_2$ sample. Figures 11B1 and B2 show the morphology of the $LiNi_{1/3}Mn_{1/3}Co_{0.19}Mg_{0.14}O_2$ sample. Figures 11C1 and C2 show the morphology of the $LiNi_{0.19}Mn_{1/3}Co_{1/3}Mg_{0.14}O_2$ sample. Figures 11D1 and D2 show the morphology of the $LiNi_{1/3}Mn_{0.18}Co_{1/3}Mg_{0.15}O_2$ sample. The samples in Figure 11A, B, and C show crystallites with flat facets, having primary particle sizes around 200 nm. The sample in Figure 11D has primary particles that are around 400 nm. The sample with Mg substituted for Mn shows the larger particle sizes.

Figure 12 shows the first charge−discharge curves of the samples. The cells were cycled between 3.3 and 4.3 V

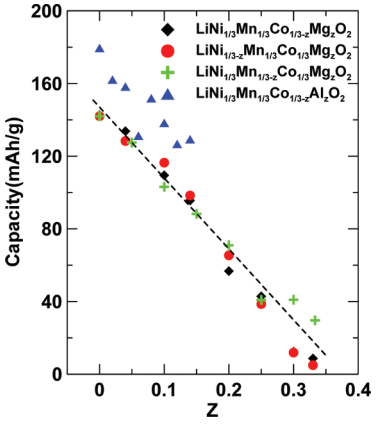

Figure 13. First discharge capacities as a function of z in $LiNi_{1/3}Mn_{1/3}Co_{1/3-z}Mg_zO_2$, $LiNi_{1/3-z}Mn_{1/3}Co_{1/3}Mg_zO_2$, $LiNi_{1/3}Mn_{1/3-z}Co_{1/3}Mg_zO_2$, and $LiNi_{1/3}Mn_{1/3}Co_{1/3-z}Al_{1/3}O_2$ (from ref [7]).

using a specific current of C/20. All the samples show smooth charge−discharge curves, and the specific capacity to 4.3 V decreases when the Mg content increases. The $z = 0$ sample has the smallest charge−discharge polarization and the smallest irreversible capacity of all the samples. Addition of Mg to the samples increases the amount of inactive (cannot be oxidized) metals in the transition metal layer and reduces the reversible capacity. Since the average transition metal oxidation state in $LiMO_2$ is M^{3+}, substituting Mg as Mg^{2+} for any of Ni, Mn, and Co, adds one inactive cation and also causes a corresponding increase in the average oxidation state of the transition metal cations. This is more severe than Al substitutions where only an inactive cation is added, and

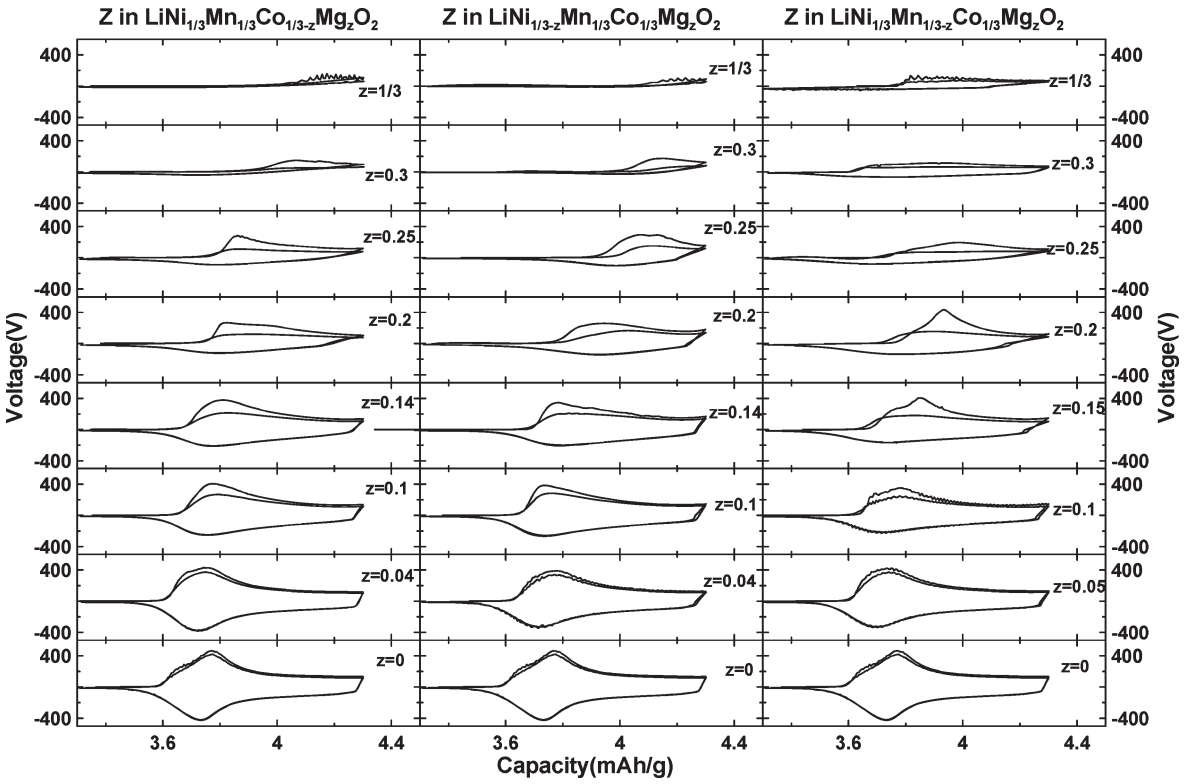

Figure 14. Differential capacity (dQ/dV) vs potential (V) of $Li/LiNi_{1/3}Mn_{1/3}Co_{1/3-z}Mg_zO_2$, $Li/LiNi_{1/3-z}Mn_{1/3}Co_{1/3}Mg_zO_2$, and $Li/LiNi_{1/3}Mn_{1/3-z}Co_{1/3}Mg_zO_2$ ($0 \leq z \leq 1/3$) cells cycled between 3.3 and 4.3 V at a rate of C/20.

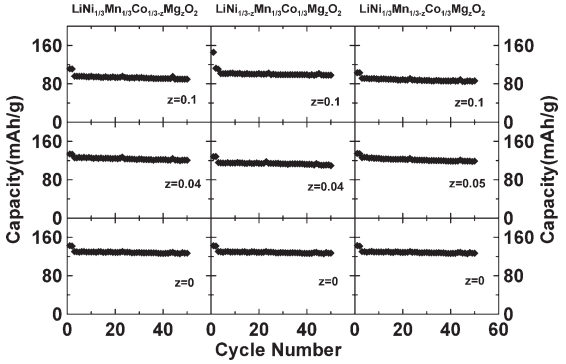

Figure 15. Specific discharge capacity vs cycle number curves of $Li/LiNi_{1/3}Mn_{1/3}Co_{1/3-z}Mg_zO_2$, $Li/LiNi_{1/3-z}Mn_{1/3}Co_{1/3}Mg_zO_2$, and $Li/LiNi_{1/3}Mn_{1/3-z}Co_{1/3}Mg_zO_2$ ($z = 0$, 0.04 (or.0.05) and 0.1) cells cycled between 3.3 and 4.3 V.

the average oxidation states of Ni, Mn, and Co are unaffected. Therefore, we expect the capacity loss with Mg content to be more rapid than the capacity loss with Al content in NMC samples.

Figure 13 shows the variation of the first discharge capacity (3.3 to 4.3 V, C/20) versus z in $LiNi_{1/3}Mn_{1/3}Co_{1/3-z}Mg_zO_2$, $LiNi_{1/3-z}Mn_{1/3}Co_{1/3}Mg_zO_2$, and $LiNi_{1/3}Mn_{1/3-z}Co_{1/3}Mg_zO_2$ ($0 \leq z \leq 1/3$). Regardless of the sample type, the capacity decreases strongly with z. The slope of the dashed line in the figure is -390 (mAh/g)/($z = 1$). Also shown in Figure 10 are results[7] for $LiNi_{1/3}Mn_{1/3}Co_{1/3-z}Al_zO_2$ for $0 < z < 0.14$. In ref 7, the specific capacity of number of Al-substituted positive electrode materials was plotted versus the Al content. It was shown that the capacity decreased with a slope of about -250 (mAh/g)/($z = 1$), which is less than that for Mg substitutions, as expected.

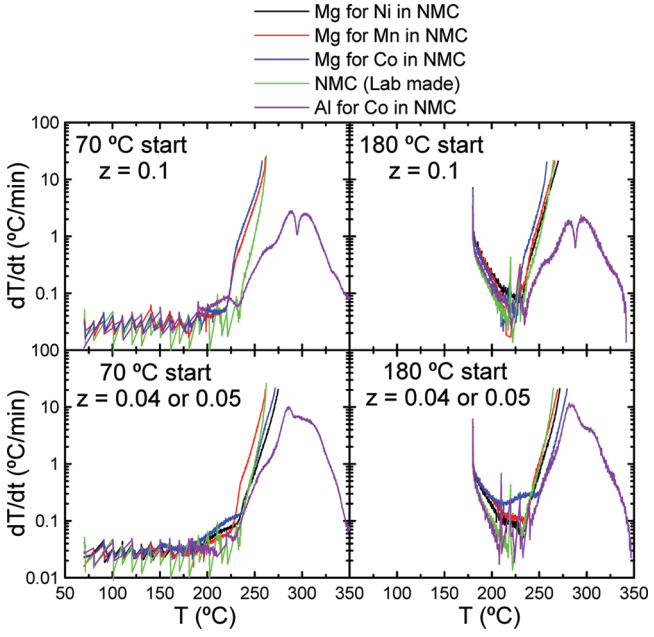

Figure 16. Self-heating rate versus temperature for the Mg substituted NMC samples charged to 4.3 V reacting with 30 mg of 1 M $LiPF_6$ EC/DEC electrolyte with starting temperatures of 70 and 180 °C. Data from NMC and Al-substituted NMC are included for comparison.

Figure 14 shows the differential capacity of the same samples described by Figure 13 plotted versus potential. For $z \leq 0.1$, the differential capacity of the samples is basically independent of which atom, Ni, Co, or Mn, was

Table 1. Rietveld Refinements Results of XRD Data and Specific Surface Areas of $LiNi_{1/3}Mn_{1/3}Co_{1/3-z}Mg_zO_2$, $LiNi_{1/3-z}Mn_{1/3}Co_{1/3}Mg_zO_2$, and $LiNi_{1/3}Mn_{1/3-z}Co_{1/3}Mg_zO_2$

chemical composition	z	a (Å)	c (Å)	Ni in Li layer	R_B	specific surface area (m^2/g)
$LiNi_{1/3}Mn_{1/3}Co_{1/3-z}Mg_zO_2$	0	2.8570	14.2149	0.0170	2.03	4.25
	0.04	2.8614	14.2342	0.0261	1.88	4.00
	0.1	2.8660	14.2391	0.0307	1.83	3.64
	0.14	2.8682	14.2511	0.0400	1.87	
	0.2	2.8742	14.2572	0.0510	1.99	
	0.25	2.8823	14.2746	0.0694	2.01	
	0.3	2.8930	14.2760	0.0816	2.58	
	1/3	2.8990	14.2893	0.0965	2.60	
$LiNi_{1/3-z}Mn_{1/3}Co_{1/3}Mg_zO_2$	0.04	2.8558	14.2219	0.0181	2.28	3.34
	0.1	2.8573	14.2319	0.0221	1.88	4.57
	0.14	2.8568	14.2345	0.0268	1.60	
	0.2	2.8554	14.2386	0.0309	2.03	
	0.25	2.8566	14.2424	0.0335	1.94	
$LiNi_{1/3}Mn_{1/3-z}Co_{1/3}Mg_zO_2$	0.05	2.8569	14.2160	0.0187	1.77	3.27
	0.1	2.8561	14.2152	0.0149	1.64	3.02
	0.15	2.8594	14.2194	0.0166	1.04	

substituted by Mg. Some differences can be observed at higher values of z.

Figure 15 shows the capacity versus cycle number for the Mg-doped NMC (with $z \leq 0.1$) cells in the voltage range between 3.3 and 4.3 V. For all the samples studied, the discharge capacity drops during the first several cycles, but remains relatively stable in the following cycles. There seems to be no advantage in cycle life caused by Mg substitution.

Figure 16 shows the self-heating rate versus temperature for the Mg-substituted NMC samples (with $z \leq 0.1$) charged to 4.3 V reacting with 30 mg of 1 M $LiPF_6$ EC/DEC electrolyte with starting temperatures of 70 and 180 °C. A 180 °C start temperature was included in an attempt to study the thermal stability of Mg-substituted NMC under forced heating conditions. Figure 16 shows that in the Mg content range studied ($z = 0-0.1$), the substitution of Mg into the layered structure of NMC doe not improve the thermal stability of the samples. The rapid exothermic reaction of NMC and of Mg-substituted NMC all begin at around 250 °C and reach the ramping rate of our ARC instrument at approximately 280 °C. Recently, we have reported the impact of Al substitution for Co on the thermal stability of NMC based electrode materials. Figure 16 gives a comparison to Al-substituted materials, where the beneficial impact of Al additions is clearly observed. According the literature,the thermal stability of charged positive electrode materials normally decreases with increasing specific surface area.[20] Therefore, the surface area is a very important factor for studies of thermal stability. Table 1 and reference 7 (Table 1 in 7) show that the surface area of these samples described byFigure 16 is 4 ± 1 m^2/g. Therefore, we do not believe that the differences between the thermal stability of Al and Mg substituted materials are caused by differences in surface area. There have been some reports that Mg substitution improves the thermal stability of layered lithium transition metal oxides based on the results of DSC testing.[12,13] However, on the basis of the ARC test results presented in this paper, it is clear that Mg substitution is not as effective as Al substitution for improving thermal stability.

(20) MacNeil, D. D.; Larcher, D.; Dahn, J. R. *J. Electrochem. Soc.* **1999**, *146*, 3596.

4. Conclusion

A full series of $LiNi_{1/3}Mn_{1/3}Co_{1/3-z}Mg_zO_2$, $LiNi_{1/3-z}Mn_{1/3}Co_{1/3}Mg_zO_2$, $LiNi_{1/3}Mn_{1/3-z}Co_{1/3}Mg_zO_2$ ($0 \leq z \leq 1/3$) samples were synthesized by the coprecipitation method. The $LiNi_{1/3}Mn_{1/3}Co_{1/3-z}Mg_zO_2$ samples were pure single phases when $0 \leq z < 0.2$, and weak peaks from Li_2CO_3 impurities were observed for $z \geq 0.2$, even though the lattice constants changed relatively smoothly over this range. The $LiNi_{1/3-z}Mn_{1/3}Co_{1/3}Mg_zO_2$ samples were pure single phases for ($0 \leq z \leq 1/3$). When Mg was substituted for Mn in $LiNi_{1/3}Mn_{1/3-z}Co_{1/3}Mg_zO_2$ pure single phase samples were observed only when $0 \leq z < 0.2$, in agreement with simple arguments based on oxidation states.

Rietveld refinements showed that Mg substitution for Co, Ni, Mn result in different degrees of cation mixing in the Li layer. The most cations move to the Li layers when Mg is substituted for Co and the least when Mg is substituted for Mn. Electrochemical studies of the $LiNi_{1/3}Mn_{1/3}Co_{1/3-z}Mg_zO_2$, $LiNi_{1/3-z}Mn_{1/3}Co_{1/3}Mg_zO_2$, and $LiNi_{1/3}Mn_{1/3-z}Co_{1/3}Mg_zO_2$ ($0 \leq z \leq 1/3$) samples were used to measure the rate of capacity reduction with Mg content, found to be about -389 (mAh/g)/($z = 1$). The reactivity of the Mg-substituted NMC samples with electrolyte was measured using accelerating rate calorimetry and compared to that of NMC and Al-substituted NMC. Unlike the case of Al substitution for Co in NMC, Mg substitution for Ni, Mn, or Co in NMC yields no significant improvement in thermal stability. Thus, it is our opinion that the value of Mg-substitutions, from a safety standpoint, is minimal.

Acknowledgment. The authors thank NSERC and 3M Canada for funding this work under the auspices of the Industrial Research Chair program. Wenbin Luo thanks the China Scholarship Council for scholarship support.